ATOMISTIC MODELING OF THE INTERACTION OF HE WITH NANOCLUSTERS IN FE—R. J. Kurtz, F. Gao, and H. L. Heinisch (Pacific Northwest National Laboratory*), B. D. Wirth (University of California, Berkeley), G. R. Odette and T. Yamamoto (University of California, Santa Barbara)

Extended abstract of a paper submitted to the Journal of Nuclear Materials as part of the proceedings of the 12th International Conference on Fusion Reactor Materials, Santa Barbara, California, December 4–9, 2005.

INTRODUCTION

Structural materials of a fusion power system will be exposed to high concentrations of He produced from nuclear transmutation reactions. Helium is essentially insoluble in metals so there is a strong tendency for it to form bubbles that can significantly degrade mechanical properties. A strategy to effectively manage He is to provide a high-density of internal interfaces to serve as He bubble nucleation sites and vacancy-interstitial recombination centers. Nanostructured ferritic alloys are being developed to provide improved creep strength and He management capability compared to conventional steels. A key characteristic of these materials is the high-density (~ 10^{24} m^{-3}) of nanometer-scale (~ 3 nm diameter) Y-Ti-O clusters. We describe molecular dynamics simulations to assess the interaction of He atoms, vacancies and He-vacancy complexes with coherent Cu nanoclusters in Fe. The potentials employed here were adjusted to explore the effect of nanocluster elastic properties on He trapping efficiency.

Computational Procedure

The Fe-Cu-He interatomic potential used here was constructed from various binary potentials obtained from the literature. All of the potentials use the Finnis-Sinclair formalism. Ackland et al. [1] have previously described the development of the Fe-Fe, Cu-Cu, and Fe-Cu potentials in detail. The Fe-He and He-He interactions have also been described previously [2]. For the Cu-He interaction the Wilson-Johnson potential was used in this work [3]. Table 1 lists important physical properties calculated from the Fe-Cu-He potential along with comparisons to experimentally measured values. The calculated properties for the bcc phase of Cu are also presented in Table 1. It should be noted that the lattice parameter of bcc Cu is ~ 3.3% larger than bcc Fe so coherent Cu nanoclusters in a Fe matrix are positive misfit particles. It is also evident from Table 1 that coherent Cu nanoclusters are elastically stiffer than Fe. Such features are considered to be representative of the physical and mechanical characteristics of Y-Ti-O nanoclusters.

To explore the effect of nanocluster elastic properties on He trapping efficiency the Cu-Cu and Fe-Cu potentials were modified so that the lattice parameter and cohesive energy for the modified fcc phase were the same as for real Cu, but the elastic constants were decreased to c_{11} = 100 GPa, c_{12} = 75.4 GPa and c_{44} = 35.3 GPa. Following an approach similar to the derivation of the original Cu potential, cubic splines were used to describe the potential functions. The form of the spline functions for the pair interaction and electron density, respectively, are as follows:

$$V(r) = \sum_{k=1}^{6} a_k (r_k - r)^3 H(r_k - r) \tag{1}$$

$$\phi(r) = \sum_{k=1}^{6} A_k (R_k - r)^3 H(R_k - r) \tag{2}$$

where H is the Heaviside step function, and r is the distance between atoms. Table 2 gives the lattice parameter and elastic constants for the new fcc and bcc phases of the modified Cu potential. The bcc

*Pacific Northwest National Laboratory (PNNL) is operated for the U.S. Department of Energy by Battelle Memorial Institute under contract DE-AC06-76RLO-1830.

lattice parameter produced by the present potential is slightly larger than that given by the Ackland et al. potential, i.e., 0.304 nm as compared with 0.296 nm. It is evident that the elastic constants for the bcc phase are much smaller than those given by the Ackland potential, which is consistent with the general tendency of fcc Cu, as shown in Table 2.

Table 1. Physical properties of Fe-Cu-He Finnis-Sinclair potential

Property	BCC Fe		FCC Cu		BCC Cu
	Calc.	Expt.	Calc.	Expt.	Calc.
Lattice parameter, nm	0.2867	0.2867 [4]	0.3615	0.3615[5]	0.2961
Atomic volume, nm^3	0.0118	0.0118	0.0118	0.0118	0.0130
c_{11}, GPa	243	230 [6]	169	169 [6]	290
c_{12}, GPa	145	135 [6]	122	122 [6]	192
c_{44}, GPa	116	117 [6]	76	75 [6]	147
Cohesive energy, eV	4.316	4.28 [7]	3.519	3.49 [7]	3.496
Point defect formation energies					
Vacancy, eV	1.70	1.6–2.2 [8–11]	1.19	1.1–1.3 [11–14]	1.32
Di-vacancy (1nn), eV	3.26	-	2.21	-	2.42
Di-vacancy (2nn), eV	3.22	-	2.42	-	2.55
Substitutional He, eV	3.25	-	2.75	-	2.54
He_1V_2 complex (1nn), eV	4.49	-	3.60	-	3.42
He_1V_2 complex (2nn), eV	4.76	-	3.98	-	3.73

Table 2. Physical properties of the modified Cu potential

Property	FCC Phase	BCC Phase
Lattice parameter, nm	0.3615	0.3041
Atomic volume, nm^3	0.0472	0.0281
c_{11}, GPa	100	198
c_{12}, GPa	75.4	103
c_{44}, GPa	35.3	66.1
Cohesive energy, eV	3.519	3.599
Point defect formation energies		
Vacancy, eV	1.00	1.67
Di-vacancy (1nn), eV	1.88	3.13
Di-vacancy (2nn), eV	2.00	3.19
Substitutional He, eV	2.68	2.67
He_1V_2 complex (1nn), eV	3.41	3.97
He_1V_2 complex (2nn), eV	3.69	4.15

For the Fe-Cu interaction, the many-body part of the cross potential is taken as the geometric mean of the elemental values, as described in detail by Ackland and Vitek [15], i.e., $\varphi_{AB}=(\varphi_{AA}\varphi_{BB})^{1/2}$. The pair component was fit to the unrelaxed single substitutional impurity (SSI) energy, and the cohesive energies and lattice parameters of fictitious L_{12} compounds, Fe_3Cu and Cu_3Fe. Based on experimental data, the heat of solution per atom can be easily calculated from the solubility limit [1], which gives the SSI energy of Cu in Fe and Fe in Cu to be 0.317 eV. Ackland et al. [1] generated the properties of the fictitious Fe_3Cu and Cu_3Fe compounds from electronic structure calculations. The cohesive energy for the present fitting is taken to be -3.9917 and -3.616 eV for Fe_3Cu and Cu_3Fe, respectively, while the lattice parameter is taken to be 0.36795 and 0.36493 nm. The cohesive energy and lattice parameter of these two

compounds, along with the experimental SSI energies, provide sufficient data for the fit of the pair component of the new cross potential.

Coherent Cu clusters embedded in a Fe matrix were used to explore how positive misfit nanodispersiods or precipitates may trap He. A 3D periodic computational cell was employed consisting of ~ 250,000 atoms. Cu nanoclusters 1–4 nm in diameter were placed at the origin of the model. Since the lattice parameter of bcc Cu is larger than Fe the Cu cluster seeks to expand, but is constrained by the surrounding Fe matrix. Consequently, models were prestrained close to the expected volume expansion of the system, estimated from $\Delta V/V=N_{Cu}(\Omega_{Cu}-\Omega_{Fe})$ where $\Delta V/V$ is the volume strain, N_{Cu} was the number of Cu atoms in the cluster, and Ω_{Cu}, Ω_{Fe} are the atomic volumes of Cu and Fe, respectively. Various He_mV_n complexes (m = 1, n = 1,2) were inserted at various distances from the Fe/Cu interface to explore the spatial dependence of the He_mV_n complex interaction with the Cu cluster. A conjugate gradient relaxation scheme was used to relax the model. The cell volume was adjusted during the relaxation to achieve zero pressure.

Results

Figure 1 shows the interaction energy between either a single vacancy (V_1) or a substitutional He atom (He_1V_1) as a function of their distance from a 2 nm diameter coherent bcc Cu cluster. The dependence of vacancy and He binding on interface character was explored by placing mono-vacancies or a substitutional He atom at different distances from either the {100} or {101} face of the Cu cluster. In this case the elastic properties of the bcc Cu nanocluster were stiffer than bcc Fe as given in Table 1. The calculated binding energies for mono-vacancies and substitutional He at the interface were nearly the same at ~ 0.58 eV. The distance dependence of the interaction energy for both types of point defects was also nearly the same, and no significant effect of interface character was found. To a first approximation the binding energies are roughly equal to the defect formation energy in bcc Fe minus the defect formation energy in bcc Cu. From Table 1 the predicted binding energies for a mono-vacancy and a substitutional He atom are 0.38 eV and 0.71 eV, respectively. It should be noted the defect formation energies given in Table 1 are computed for the pure metals at zero temperature and pressure, hence, the defect formation energies in the Cu nanocluster and in Fe near the nanocluster will be different due to the compressive stress state that exists in these regions.

Figure 2 presents the defect-nanocluster interaction energy results for both di-vacancies (V_2) and He/di-vacancy complexes (He_1V_2) in the vicinity of a 2 nm coherent Cu nanocluster that was stiffer than Fe. Both first nearest neighbor (1nn) and second nearest neighbor (2nn) di-vacancy configurations were considered. The dependence of binding energy on interface character was also examined and found not to be significant. The binding energies of di-vacancies and He/di-vacancy complexes were nearly the same at ~ 0.85 eV near the interface. Similar to the mono-vacancy and substitutional He, the binding energy for di-vacancies and He/di-vacancy complexes can be predicted from the difference in their defect formation energies in Fe and Cu. For 1nn V_2 and He_1V_2 defects the binding energies predicted from the data in Table 1 are 0.84 and 1.07 eV, respectively. Similarly, for 2nn V_2 and He_1V_2 defects the predicted binding energies are 0.67 and 1.03 eV, respectively. The predicted binding energies are fairly close to the calculated value, which is somewhat unexpected given that these defects simultaneously reside in both the Cu nanocluster and in the Fe matrix.

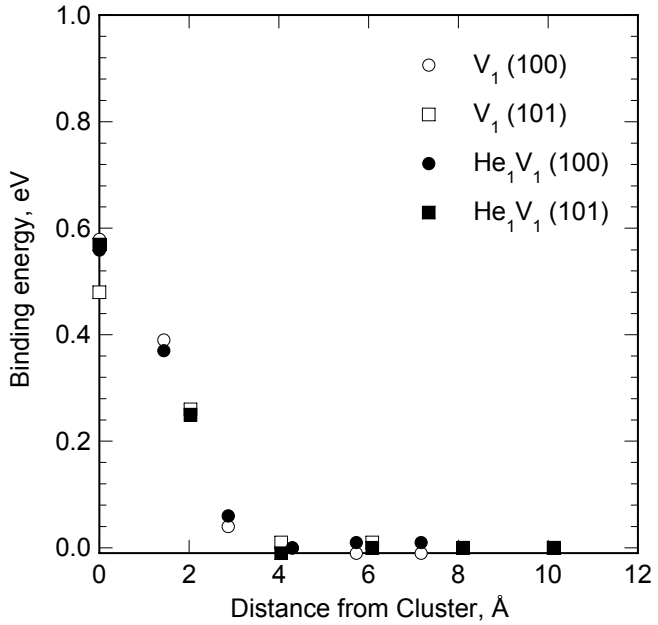

Fig. 1. The interaction energy between a single vacancy (V_1) or a substitutional He atom (He_1V_1) and a 2 nm coherent bcc Cu cluster in Fe as a function of the distance from either the {100} or {101} face of the Cu cluster. The Cu cluster is elastically stiffer than Fe.

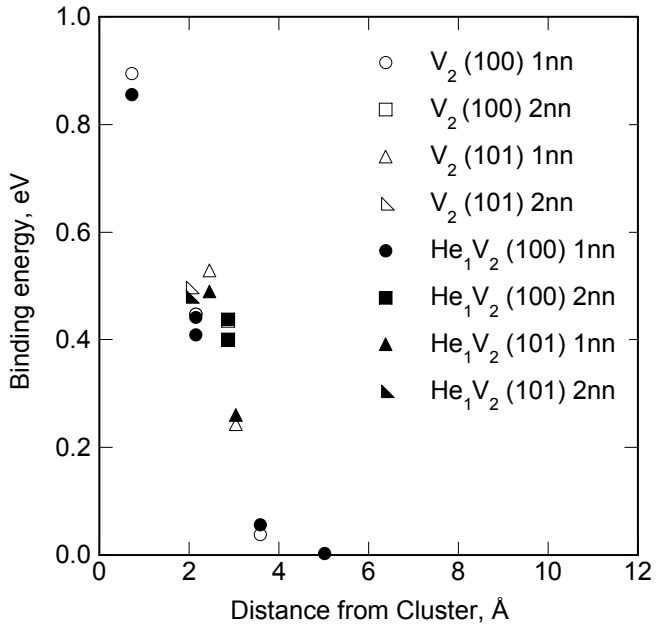

Fig. 2. The interaction energy between a di-vacancy (V_2) or a He/di-vacancy (He_1V_2) complex as a function of distance from a 2 nm coherent bcc Cu cluster in Fe. Di-vacancy configurations are either first nearest neighbor (1nn) or second nearest neighbor (2nn). The Cu cluster is elastically stiffer than Fe.

The dependence of the 1nn He_1V_2 complex binding energy on nanocluster size was examined. The He_1V_2 complex was more weakly bound to a 1 nm diameter nanocluster (~ 0.55 eV) than to clusters ranging from 2–4 nm. The binding energy was approximately the same for 2–4 nm diameter clusters (~ 0.85 eV). It is not surprising that the He_1V_2 complex is more weakly bound to the 1 nm cluster since this nanoparticle consists of only 59 Cu atoms. Most of the Cu atoms in the nanocluster have Fe atoms for neighbors consequently the properties of defects near the nanocluster will be dominated by the defect properties of Fe.

Figures 3 and 4 display results analogous to those shown in Figs. 1 and 2 except that the interatomic potentials were modified to produce a bcc phase that has about the same lattice parameter as bcc Cu but with elastic properties softer than Fe. Note the cohesive energy for the modified fcc phase is the same as fcc Cu, but the cohesive energy of the modified bcc phase is about 0.1 eV greater than the original bcc Cu. The larger cohesive energy may partially account for the 0.35 eV increase in the mono-vacancy formation energy. The results clearly show that vacancies and He-vacancy complexes are more weakly bound to the modified bcc nanoclusters. In addition, mono-vacancy binding energies (0.28–0.35 eV) were lower than substitutional He binding energies (0.39-0.49 eV). The defect formation energy data given in Tables 1 and 2 suggest this trend. The vacancy formation energy in the modified bcc phase is only 0.03 eV smaller than bcc Fe, so weaker binding of mono-vacancies is expected. Similarly, the substitutional He formation energy in the modified bcc phase is 0.13 eV greater than in bcc Cu, so weaker binding would be anticipated. Further, the differences in defect formation energies suggest that substitutional He atoms would be bound more strongly than single vacancies to the modified bcc phase as shown in Fig. 3. Di-vacancies and He_1V_2 complexes were also more weakly bound to the modified bcc phase, which results from the increased defect formation energies in the modified bcc phase relative to bcc Cu (see Tables 1 and 2). Differences in defect formation energy predict that di-vacancies should be more weakly bound to the nanocluster than He_1V_2 complexes, but the results displayed in Fig. 4 indicate the opposite was observed.

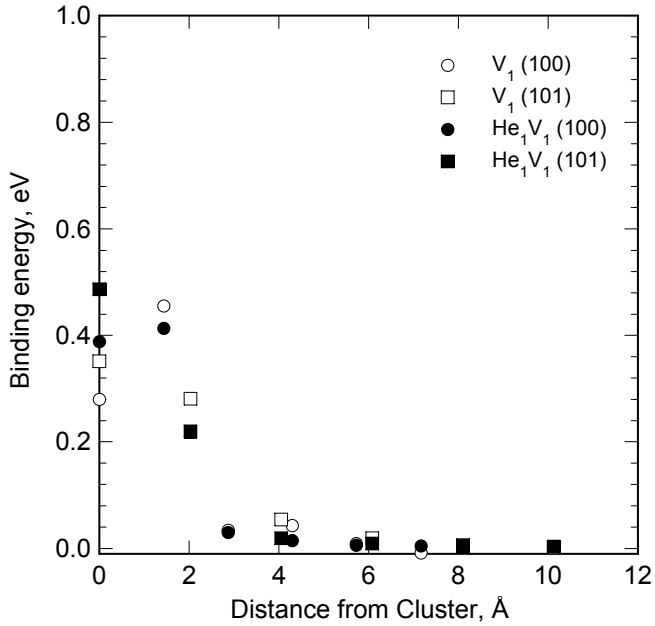

Fig. 3. The interaction energy between a single vacancy (V_1) or a substitutional He atom (He_1V_1) as a function of distance from a 2 nm cluster in Fe. The interatomic potential for Cu was modified to make the nanocluster elastically softer than the Fe matrix.

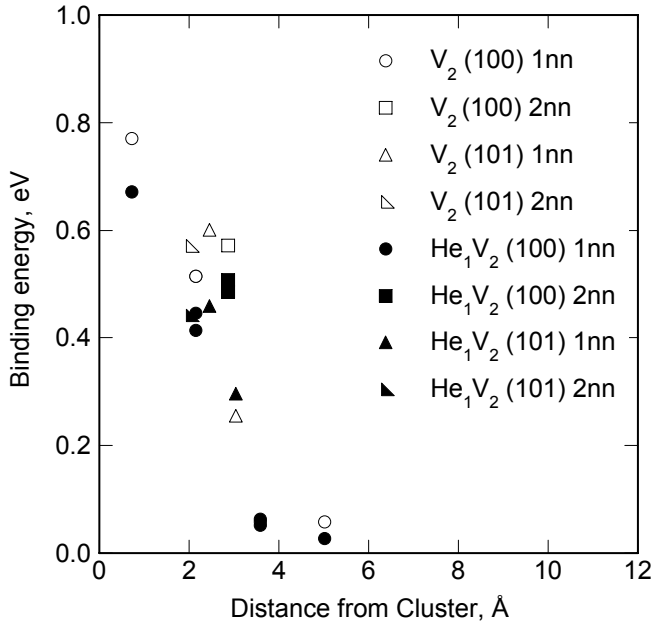

Fig. 4. The interaction energy between a di-vacancy (V_2) or a He/di-vacancy (He_1V_2) complex as a function of distance from a 2 nm Cu cluster in Fe. Di-vacancy configurations are either first nearest neighbor (1nn) or second nearest neighbor (2nn). The interatomic potential for Cu was modified to make the nanocluster elastically softer than the Fe matrix.

Conclusions

Atomistic computer simulations were used to explore the effectiveness of coherent nanoclusters for trapping He in a Fe matrix. All point defect complexes considered in this study were bound to 2 nm Cu clusters with binding energies ranging from 0.50–0.58 eV for single vacancies and substitutional He atoms. Di-vacancies and He/di-vacancy complexes were more strongly bound with binding energies of ~ 0.85 eV. He/di-vacancy complex binding energy increases with cluster size and reaches a maximum of ~ 0.85 eV for clusters ≥ 2 nm in diameter. Point defects were not as strongly bound to nanoclusters elastically softer than Fe when compared to binding energies to nanoclusters elastically stiffer than Fe. Differences in point defect formation energies were likely responsible for the different binding energies observed rather than the specific elastic properties of the nanoclusters. The point defect "capture radius" for 2 nm Cu clusters was about 0.4 nm, independent of defect formation energy differences or nanocluster elastic properties.

References

[1] G. J. Ackland, D. J. Bacon, A. F. Calder, and T. Harry, "Computer Simulation of Point Defect Properties in Dilute Fe-Cu Alloy Using a Many-Body Interatomic Potential," Philos. Mag. A. 75(3) (1997) 713–732.

[2] R. J. Kurtz and H. L. Heinisch, "The Effects of Grain Boundary Structure on Binding of He in Fe," J. Nucl. Mater. 329–333 (2004) 1199–1203.

[3] W. D. Wilson and R. D. Johnson, "Rare Gases in Metals, Interatomic Potentials and Simulation of Lattice Defects," P. C. Gehlen, J. R. Beeler, Jr., and R. I. Jaffee (eds.), Plenum Press, New York (1972) 375–390.

[4] R. Kohlhaas, P. Dunner, and P. N. Schmitz, "The Temperature-dependance of the Lattice Parameters of Iron, Cobalt, and Nickel in the High Temperature Range," Z Angew Physik 23(4) (1967) 245–249.

[5] M. E. Straumanis and L. S. Yu, "Lattice Parameters, Densities, Expansion Coefficients, and Perfection of Structure of Cu and Cu-In Alpha-Phase," Acta Crystallogr. 25A (1969) 676–682.

[6] Landolt-Boernstein, Numerical Data and Functional Relationships in Science and Technology, New Series, Group III, Vol. 2, Springer-Verlag, Berlin (1979).
[7] C. Kittel, Introduction to Solid State Physics, Sixth Edition, John Wiley & Sons, Inc., New York (1986) 55.
[8] K. Fuederer, K.-P. Doering, M. Gladisch, N. Haas, D. Herlach, J. Major, H.-J. Mundinger, J. Rosenkranz, W. Schafer, L. Schimmele, M. Schmolz, W. Schwarz, and A. Seeger, "Vacancy Formation in Thermal Equilibrium in Ferromagnetic Iron and Cobalt Studied by the Spin Rotation of Positive Muons," Mater. Sci. Forum 15–18 (1987) 125.
[9] L. De Schepper, G. Knuyt, L. M. Stals, D. Segers, L. Dorikens-Vanpraet, M. Dorikens, and P. Moser, "Migration and Formation of Vacancies in α-Iron," Mater. Sci. Forum 15–18 (1987) 131.
[10] H.-E. Schaefer, K. Maier, M. Weller, D. Herlach, A. Seeger, and J. Diehl, "Vacancy Formation in Iron Investigated by Positron Annihilation in Thermal Equilibrium," Scr. Metall. 11 (1977) 803.
[11] H.-E. Schaefer, "Investigation of Thermal Equilibrium Vacancies in Metals by Positron Annihilation," Phys. Status Solidi (a) 102 (1987) 47.
[12] S. Nanao, K. Kuribayashi, S. Tanigawa, M. Mori, and M. Doyama, "The Measurement of the Formation Energy of a Vacancy in Cu by Positron Annihilation," J. Phys. F 3(1) (1973) L5–L8.
[13] H. Fukushima and M. Doyama, "The Formation Energies of a Vacancy in Pure Cu, Cu-Si, Cu-Ga, and Cu-Mn Solid Solutions by Positron Annihilation," J. Phys. F 6(5) (1976) 677–685.
[14] O. Le Bacq, F. Willaime, and A. Pasturel, "Unrelaxed Vacancy Formation Energies in Group-IV Elements Calculated by the Full-Potential Linear Muffin-Tin Orbital Method: Invariance with Crystal Structure," Phys. Rev. B 59(13) (1999) 8508.
[15] G. J. Ackland and V. Vitek, "Many-Body Potentials and Atomic-Scale Relaxations in Noble-Metal Alloys," Phys. Rev. B 41 (1990) 10324–10333.